RSC Advances

ROYAL SOCIETY OF CHEMISTRY

www.rsc.org/advances

RSC Advances

ARTICLE

Fabrication of Field-Effect Transistors and Functional Nanogenerators using Hydrothermally Grown ZnO Nanowires

Received 00th January 20xx,
Accepted 00th January 20xx

DOI: 10.1039/x0xx00000x

www.rsc.org/

C. Opoku*[a], A. S. Dahiya[a], F. Cayrel[a], G. Poulin-Vittrant[b], D. Alquier[a], N. Camara[a]

The present work demonstrates the production of single crystalline ZnO nanowires (NWs) using the low temperature hydrothermal process and their integration as the active channel material and piezoelectric elements in single NW field-effect transistors (FETs) and functional nanogenerators (NGs), respectively. Even though hydrothermally grown ZnO NWs show high levels of excess free carriers >>10^{18}/cm^3, we show that an optimized thermal annealing process at just 450^{o}C in atmospheric air sufficiently reduces this level to around ~3.7x10^{17}/cm^3. The excess free carrier suppression is verified by assessing the field-effect transport behaviour in a single NW FET. The single device is found to exhibit good performance metrics, including low off-state current (pA range), high on-state current (in the 10s of µA range) and moderate effective mobility (~10cm^2/V-s). The functional NGs are based on vertically grown ZnO NWs with ~7µm thick Polydimethylsiloxane (PDMS) polymer matrix. We show that *a* NG incorporating annealed ZnO NWs can continuously generate higher output voltages and power compared to a reference device based on as-grown ZnO NWs. This included peak output voltage of ~109mV and an output power density of ~16µW/cm^3. We envisage that this approach of thermal annealing may find practical applications in other areas of hydrothermal ZnO NW research, including high performance NW FETs and piezoelectric energy harvesters.

Introduction.

Ambient noise represents a source of energy inexorably entwined with the living world. Such energy sources may take the form of sunlight, mechanical vibrations, gas flow, irregular motion etc.. The development of new technologies able to siphon and convert even a fraction of this wasted energy into electricity represents a novel approach to reducing our ever increasing reliance on fossil fuels[1-3]. These energy harvesters can range from the well developed photovoltaic (PV) cells to the unconventional piezoelectric nanogenerators (NGs). Advancements in the synthesis of piezoelectric nanomaterials is offering enormous potential in this area of research and unlike traditional energy harvesters, piezoelectric generators incorporating NWs can continuously generate electricity, unabated by ambient conditions[3-5]. Hydrothermally grown ZnO nanowires (NWs) have emerged as viable material candidates for this technology due to their unique properties, offering two fold advantage over other piezoelectric modules: i) the performance of inorganic piezoelectric modules and ii) the ease of processing, similar to most organics piezoelectrics[5-7]. These unique features of the material have resulted in demonstrations of various prototypical self-powered system, including on-board charging of portable electronics, environmental monitoring and implantable sensors[8-10]. Among the various NG architectures proposed, the vertical integrated nanogenerator (VING) is the most developed due its relative ease of fabrication[5, 8]. The structure is based on forming Schottky contacts between a conductive surface/substrate and the piezoelectric semiconducting ZnO NW arrays[11]. A non-conductive polymer typically forms a composite matrix with the NWs and metallic layers are deposited on the matrix surface to define the active working area. In operation, application a force on the top surface of the active region generates an apparent voltage potential gradient as a result of direct piezoelectric effect[6,11,12]. This voltage potential can then be used to drive electrical charges through an external load via capacitive coupling[6]. With this design, truly impressive electrical outputs can be expected, including an open circuit voltage, short circuit current and an instantaneous power of ~58V, 134µA and 0.78 W/cm^3, respectively[5,8]. Despite the potential of hydrothermally grown ZnO NWs as possible piezoelectric elements in energy harvesters, detailed understand of the underlying mechanism accounting for energy generation is still not fully understood, since the level of the excess free carries in the material has been theorized to completely neutralise the induced piezoelectric potential beyond 10^{18}/cm^3 [11]. Another factor limiting hydrothermal ZnO NW-based NG performance is the formation reliable Schottky contacts, which can offer additional electrical isolation[11,13]. Although recent reports have shown that such limitations can be minimized by: i) passivation of hydrothermal ZnO NW's surface using solution processable p-type polymers, ii) annealing hydrothermally grown ZnO NWs in an oxidative environment

[a] Université François Rabelais de Tours, CNRS, GREMAN UMR 7347, 16 rue Pierre et Marie Curie, 37071 TOURS Cedex2, France.
[b] Université François Rabelais de Tours, INSA-CVL, CNRS, GREMAN UMR 7347, 3 rue de la Chocolaterie, CS 23410, 41034 BLOIS, France

(>350°C) and iii) isolation of the ZnO NW's base and tips from external electrodes using insulating layers[5,6,8,14]. Whilst passivation by p-type polymers may lead to the formation of p-n junctions with hydrothermally grown ZnO NWs, isolation of ZnO NW using insulating layers have been shown to suppress the leakage currents that can degrade device performance[10,14]. Moreover, the exact processes by which the above two methods are able to suppress the piezopotential screening caused by excess carriers in hydrothermal ZnO NWs have not been sufficiently explained[6,8,10,14]. The present work is not intended to produce devices that outperform reported work elsewhere. Instead, we present a study of hydrothermal ZnO nanowire applications targeting electronics and piezoelectric energy harvesters. By annealing hydrothermally grown ZnO NWs at just 450°C, we show that high performance single ZnO NW field-effect transistors with extracted carrier concentration (n_e) of around $3.7x10^{17}/cm^3$ can be obtained. The modified ZnO NWs were also employed as active piezoelectric elements for the assembly of NGs. Devices incorporating the modified ZnO NWs are characterized, revealing much enhanced output power of around a factor of 4 higher than a reference device containing pristine hydrothermal ZnO NWs.

Results and discussions.

ZnO nanowire synthesis. The ZnO nanowires used in this work were synthesized by the hydrothermal process at around 100°C. The growth was carried out separately on Au/Ti-Si and ZnO nanocrystals seeded Si substrates. For the growth on Au/Ti-Si substrates, the reaction nutrient solution was based on 100mmol zinc nitrate hexahydrate ($Zn(NO_3)_2{\cdot}6H_2O$), 100mmol hexamethylenetetramine ($C_6H_{12}N_4$), and 10mmol ammonium hydroxide ($NH_4{\cdot}4OH$, 30% wt%, reagent grade, Sigma Aldrich).

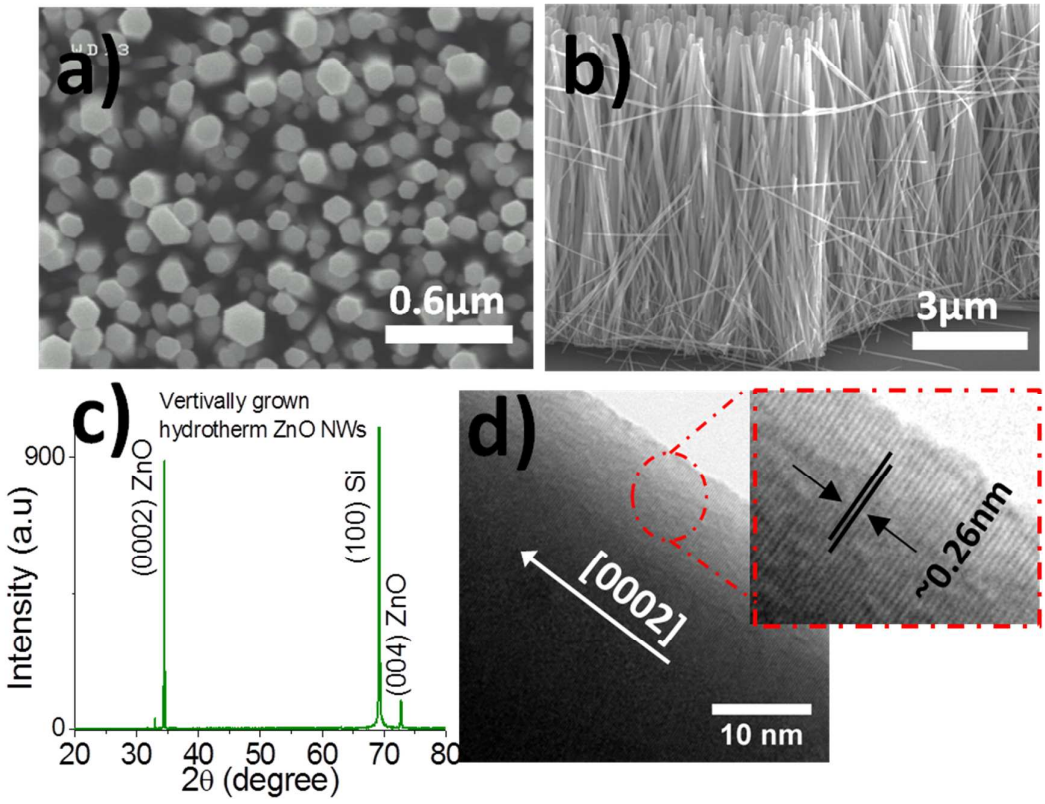

Figure 1. a-b) Family of SEM images of the resulting ZnO NW growth on a ZnO nanocrystal seeded Si substrate. c-d) XRD spectrum and HRTEM data of as-grown ZnO NWs.

Similar growth nutrients were also employed for NW growth on ZnO nanocrystal seeded substrates, except that here, ammonium hydroxide was substituted by Polyethylenimine (PEI, end-capped, 800g/mol molecular weight) at 5mmol. Substrates were sealed face down in a Teflon lined stainless steel Autoclave reactor containing ~60mL growth nutrients and placed inside a preheated convection oven at ~100°C for 12-15 hrs for reaction maturity. After the synthesis, substrates were retrieved and rinsed thoroughly in warm DI-water (~50-60°C), followed by baking at around ~100°C on a hotplate (~10min). Fig. 1 shows representative scanning electron microscope (SEM) images, x-ray diffraction (XRD) and high-resolution transmission electron microscope (HRTEM) data of as-grown ZnO NWs. From Fig. 1a, it can be seen that we obtained highly dense ZnO NW arrays. The ZnO NWs are also observed to

exhibit excellent structural orientation, perpendicular to the growth substrate. Several SEM images were assessed, revealing typical NW density, diameter and length on the different substrates to be around ~74.5 NW/μm^2 ±6.5, 115nm ±64, 0.97μm ±0.34 (Au/Ti-Si substrates) and ~200 NW/μm^2, 59nm ±44nm and 1.8μm ±0.5μm (ZnO nanocrystal seeded substrates). Longer NWs (> 9μm) were also obtained by replenishing nutrient solutions several times during synthesis (Fig. 1b). Although, this approach of nutrient replenishing was also found to y produce NWs with larger average diameters (~200nm ±100). From the XRD data (Fig. 1c), we observe two dominant peaks cantered at 2θ = 34.4^o and 72.5^o, corresponding to the (0002) and (0004) planes of a highly c-axis orientated wurtzite ZnO. Additional peak appearing at 69.1^o, were successfully assigned to the Si (100) growth substrate. The ZnO NW growth direction was further confirmed by HRTEM, as shown in Fig. 1d. From this data, it can be seen that the ZnO NW exhibited well ordered interference patterns, with spacing between adjacent planes of around ~0.26nm. This feature of the material is consistent with that of wurtzite ZnO nanomaterial grown along the [0001] direction[15].

Single ZnO nanowire field-effect transistor study

Electrical transport studies were conducted on single NW devices to assess the possibility of suppressing the excess free carriers in our hydrothermally grown ZnO NWs by thermal annealing. Such device were constructed as bottom-gate, top-contact FET structures on highly degenerate Si (p^{++}) substrates with ~170nm thick thermally grown SiO_2 on top. The NWs were first transferred from growth the substrates into anisole solvent. A brief agitation in a sonic bath was then performed to ensure adequate NW suspension in anisole. NW formulation was subsequently applied over clean SiO_2/Si substrates by solution casting methods. Prior to forming contacts to individual ZnO NWs, substrates containing ZnO NWs were transferred to a quartz tube furnace, where they were annealed at various temperatures ranging from 350^{o}C to 550^{o}C. Devices were finally finished by patterning Al/Ti (~200/10nm) source and drain (s/d) contacts onto the ends of individual NWs (electron beam lithography, lift-off). Overall, we find that 450^{o}C and 550^{o}C annealing provided sufficient passivation of the oxygen vacancies in our hydrothermally grown ZnO NWs. 350^{o}C annealing on the other hand was found to offer insufficient passivation and hence such devices will not be discussed in the work. The single ZnO NW devices were characterized in ambient air on a Cascade Microtech Summit 11k probe stage using a single source measurement unit (Keithley 2636A). We show in Fig. 2a-b, the schematic and the representative SEM image of the fabricated single NW devices. From the SEM images, it can be seen that the ZnO NWs were effectively sandwiched between metallic s/d contacts and substrate for maximum contact area. Fig. 2c-d shows the room temperature transfer and output scans for a 450^{o}C annealed, ~200nm diameter single ZnO NW device with a channel length (L) of around ~6.4 μm. From these data, it can be seen that increasing the gate voltage (V_G) towards positive values resulted in drain current (I_D) increase. This behaviour of the device is consistent with that of an n-channel accumulation-type FET. Within the measured V_G range, we extracted a low off-state current (in the sub pA range at $V_G \approx$ -46.2V) and high-on state current of ~10μA (at V_G = 20V). From the logarithmic ratio of the off- and on-state currents (Fig. 2c), a high on/off ratio of ~10^8 was deduced. In the subthreshold regime, we extracted the subthreshold slope (s-s) to be around ~633mV/dec. These characteristics were not extractable from pristine and/or 350^{o}C annealed ZnO NW based FETs. Moreover, the extracted parameters compare favourably with reported data elsewhere for thermally modified single ZnO NW FETs[16]. Although, it must be noted that the hydrothermal ZnO NWs from ref:[16] were annealed at much higher temperatures (600^{o}C, 15min) compared to the present work.

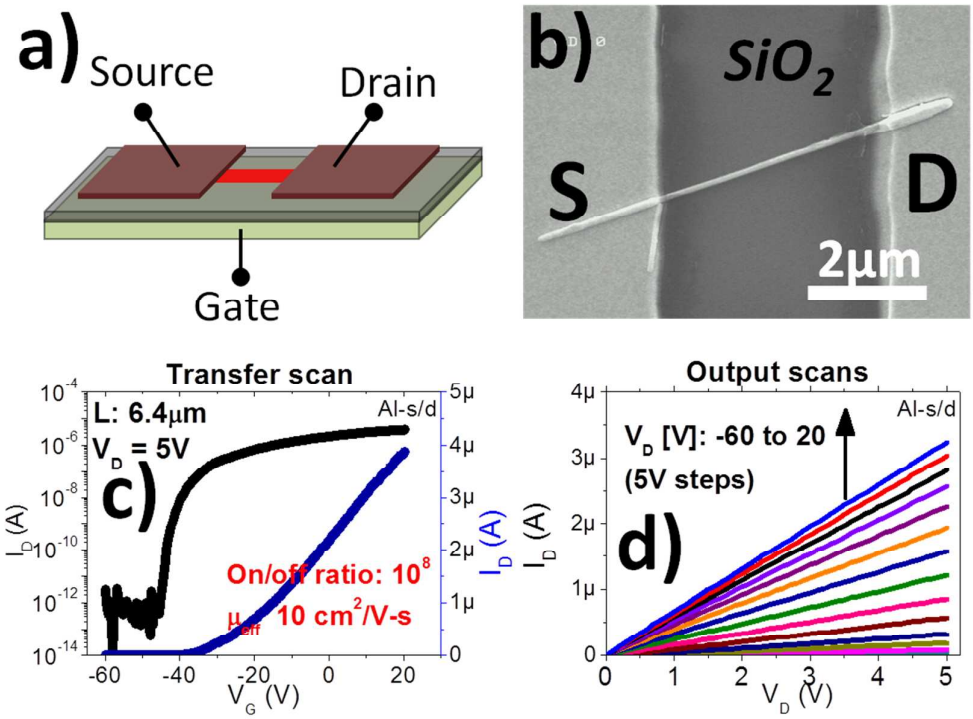

Figure 2. a) Schematic illustration of the single ZnO NW FET structures. b) SEM image of a representative single ZnO NW device. c) Transfer scan in both *semi-log* (left) and *lin-lin* scale (right). d) Family of output scans at V_G = -60 to 20V (5V steps) for the same device.

From the output scans, a near linear I_D progression at low drain voltages can be observed (Fig. 2d). The non-zero threshold voltage (V_T) of ~-26V (Fig. 2c) can sufficiently explain the lack of saturation observed in the output scans. This V_T value may also hint at the presence of residual carriers that cannot be completely eliminated even at 450°C annealing. Additionally, the existence of interfacial states, especially those present at the ZnO-SiO_2 interface are expected to shift V_T towards higher negative V_G values. In either case, the ZnO NW channel may be populated by electrons at V_G = 0V, requiring high negative voltages at the gate for channel pinch-off[17]. Nonetheless, using the extracted V_T value, an effective carrier concentration in the channel can be estimated from the expression[18]:

$$n_e \approx \frac{C_{NW} V_T}{2\pi r^2 L} \quad (1)$$

where

$$C_{NW} \approx \frac{2\pi\epsilon_o\epsilon_r L}{cosh^{-1}\left(\frac{r+d_{ox}}{r}\right)} \quad (2)$$

From the above expressions (Equation 1 and 2), C_{NW} represents the channel capacitance based on the cylinder-on-plate approximation (~0.87fF), L is the channel length, r is NW radius (~100nm), ε_o, ε_r, d_{ox} and L represent the dielectric constant of free space, relative permittivity and thickness of the SiO_2 gate dielectric, respectively. Using Equation 1, a conservative estimate for n_e was calculated to be around 3.7x10^{17}/cm^3. Whilst this parameter was not extractable in single NW FETs based on as-grown and 350°C annealed hydrothermal grown ZnO NWs, a n_e of around 1.7x10^{16}/cm^3 was obtained in a representative device based on 450°C annealing (see Fig. S5, supporting information). The modified MOSFET model for mobility μ_{eff} $\left(\approx \frac{\partial I_D}{\partial V_G} \times \frac{L^2}{V_D C_{NW}}\right)$ in the linear regime was applied for the estimation of an effective carrier mobility of around 10cm^2/V-s in this device. This value compares favourably with similar ZnO NW device structures based on much higher temperature synthesis [18,19]. From our previous discussions, it can be seen that the extracted n_e value in the 450°C thermally modified NW device is still highly promising for piezoelectric energy harvesting applications, where low to moderately doped ZnO NW materials are required [11]. As we show in later sections of this work, NGs incorporating such ZnO NWs are able to generate comparatively higher output voltages and power compared to a reference device based as-grown hydrothermal ZnO NWs.

Nanogenerator assembly and characterisation.

In this section, we compare the performance of a NG based on 450°C the thermally modified ZnO NWs with an unmodified NW NG. Such devices were constructed using vertically grown ZnO NWs on Au/Ti-Si substrates. Assessment of several SEM images were also found to show no morphological variations between the as-grown and the 450°C thermally modified ZnO NW arrays (Fig. S1 and S3,

supporting information). To assess the quality of aligned ZnO NW arrays after thermal annealing, x-ray diffraction was also performed, revealing highly c-axis orientated ZnO NW arrays (see Fig. S2 and S4 from supporting information). To fabricate such devices, ZnO NW arrays were first encased in ~7µm thick PDMS to form ZnO NW-polymer matrices . Unlike to other polymers proposed for NG assembly, PDMS is a highly transparent elastomer with excellent moisture barrier properties.. Moreover, the material also exhibits low shrinkage after cross-linking[20]. A schematic of the process flow employed for the assembly of the present NGs can be found in Fig. 3a. The PDMS mixture was prepared by mixing PDMS curing agent, toluene and PDMS base at a mass ratio of 1:3:10. The mixture was dispensed onto NW substrates and a degassing step was performed under low vacuum (~25 Torr, ~30-60min) to remove the air bubbles from the mixture. Following this step, excess PDMS was removed from substrate surface by spin coating at 3000rpm for ~60s. Substrates were then baked at ~100^{o}C (1hr) to cross-link the PDMS (Fig. 3a(1)-(4)). Devices were finally finished by the evaporation of Al (~400nm) on the top surfaces of the structures to define the active working area for the devices (2.5cm^2), as shown in Fig. 3a(5). To ensure that this region could be strained uniformly during testing, double sided Al coated (~200nm) glass substrates were also bonded on top of device active areas (Fig. 3a(6)). Copper wires were subsequently attached to the top and bottom conductive surfaces of the NGs (by silver paste) to ensure facile probing. An optical image of a finished NG is shown Fig. 3b. The quality of the resulting ZnO NW-polymer matrix layers were assessed by cleaving some of the NGs followed by imaging under SEM. Fig. 3c-d shows a representative cross-sectional SEM image, revealing the internal structure of the NGs. From Fig. 3c-d, several important observations can also be made. Firstly, it can be seen that we obtained excellent ZnO NW-PDMS composite structures, whereby the ZnO NW are effectively sandwiched between the different layers (Fig. 3c-d).

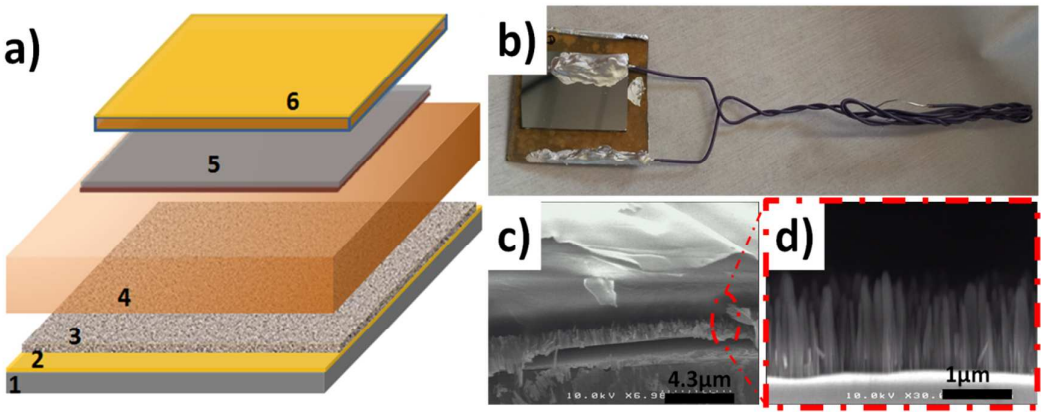

Figure 3. Schematic of the ZnO NW based NG assembly steps. 1-3 correspond to ZnO NW growth, 4 represents the PDMS polymer encapsulation step, 5-6 shows top electrode deposition and bonding of conductive glass substrates, respectively. b) Photograph of a completed NG device, c-d) cross-sectional SEM image of a finished device ZnO NW based NG.

Notably, it can also be observed that the ZnO NWs maintained their excellent orientation even after the PDMS curing step (Fig. 3d). Finally, the PDMS is clearly shown infiltrate the voids between adjacent ZnO NWs on the substrates (Fig. 3d). Such features are expected to significantly minimised the undesirable effects that can degrade NG's performance (e.g. electrical shorting between adjacent ZnO NWs, leakage current at the top electrode-polymer-ZnO NW interface and structural failure of ZnO NWs during testing) [11]. The thickness of the PDMS atop the NWs was estimated from SEM images to be around 7 ±0.5 µm. This thickness of the polymer layer atop the ZnO NWs is comparatively larger than the literature data for similar NGs based on other polymers like PMMA or PEDOT:PSS (~0.2-2µm) [5,6]. It is anticipated that these differences may lead to lower degree of capacitive coupling. This in turn, may lead to lower output performance in our devices[11]. Although, the 7µm thick polymer matrix used in this work is significantly lower than the 200µm thick PDMS from ref:[9], where high NG output characteristics were reported, including an open circuit voltage and output power of 8V and ~5.3mW/cm^3, respectively.

Influence of thermal annealing on nanogenerator output. The fabricated NGs were characterised on a custom built test-bench comprising of a mechanical shaker (LDS V406) equipped with a ridged aluminium actuator arm, as shown in Fig. 4a. The amplitude and frequency of the shaker was controlled via an Agilent 33250 function generator and a LDS PA100E power amplifier was used to drive the shaker. The actuator arm was attached to the reciprocating shaker platform at one end and a height adjustable screw was inserted through it at the opposite end. To avoid excessive damage to the NGs during testing, the screw tip was also insulated by soft styrene-butadiene rubber. The NGs were then firmly fixed onto a solid aluminium block using double sided adhesive tape. The screw tip was positioned over the active region of the NG, without making contact. Whilst the exact forces subjected to the NGs were unknown during testing, a constant

output voltage (~1V) was maintained on a commercial PZT disc buzzer positioned between two insulating glass plates under the NGs. Finally, all NG output responses were recorded on an Agilent DSO5054A oscilloscope via a voltage probe. The output voltage response for representative NGs based on pristine and thermally modified ZnO NWs using the current experimental setup can be found in Fig. 4b-c. From these data, it can be seen that the input voltage signal actuating the shaker was a square wave with a $2V_{pp}$ amplitude and a periodicity of 0.1s. Whilst the neutral position of the shaker was unknown, it can be seen from the measured data that both NGs were subjected to short impulsive forces, since abrupt positive voltages are immediately followed by sudden negative voltage spikes only in the lowest potions of shaker input signal (Fig. 4b-c). We also note that a measurable output response is still observed from the NG with pristine NWs (Fig. 4b). This behaviour of the device presumably suggest that the piezoelectric potential in this device may not be completely neutralised by the high density of carriers in the material (Fig. 4a). For this device, the measured voltages in the positive and negative cycles were around 56 ±2.4 mV and -43 ±3.2 mV, respectively. The same parameters were extracted be ~109 ±6 mV and -80 ±1.5 mV (Fig. 4b) in the thermally modified ZnO NW device. The higher output voltages in the latter case can be expected due to the greatly reduced carrier screening in the thermally modified ZnO NWs in this device. Although we acknowledge that the measured output voltages in the present devices are significantly lower than the 37V from ref:[5]. Such different may be explained by the markedly different measurement conditions employed in present work (e.g. resistive and mechanical loading conditions as well as the mechanical properties of the polymers used). Moreover, by using ZnO NWs from identical hydrothermal synthesis processes and identical testing conditions, we are able to show that the NGs incorporating thermally annealed ZnO NWs can produce around a factor of two higher output voltages than a reference device with pristine NWs.

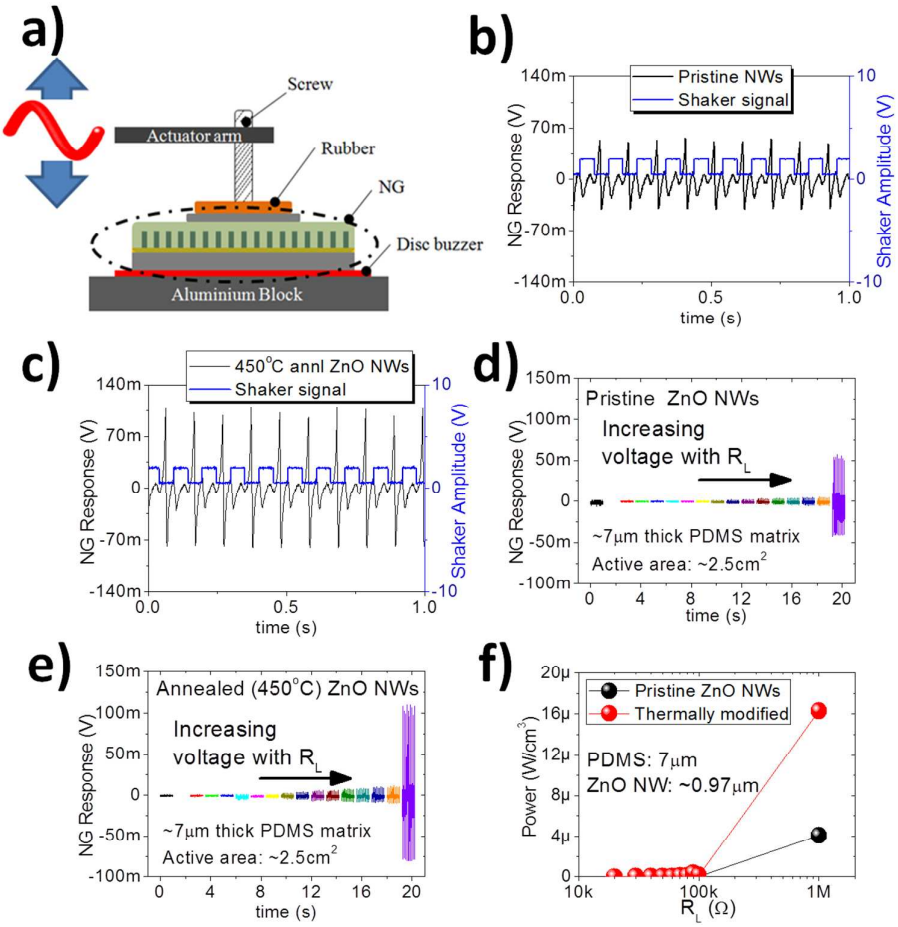

Figure 4. a) Schematic of the test bench. b-c) output voltage response from a nanogenerator based on as-grown (b) and 450°C thermally modified ZnO NWs. d-e) measured output voltage vs. resistive load for the same devices. f) Power density vs. resistive load for the device.

Energy harvesters generally present a source impedance to their load circuits and in operation, maximum power output power is obtained when the load impedance is matched to that of the harvester [6].

To assess the impact of resistive loading on the measured NG output characteristics, we conducted a series of experiments, in which the load resistors (R_L) were varied between 0.6MΩ to 1MΩ.

Experimental data resulting from the various R_L can be found in Fig. 4d-e. From these data, it can clearly be observed that the output voltages for both devices increases with increasing of R_L. Notably the NG incorporating the thermally modified ZnO NWs consistently generated higher output voltages than the device based on unmodified NWs. A measure of the power output as a function of R_L can be obtained from the expression[6]:

$$P_v = \left(\frac{P_A}{d}\right) \quad (3)$$

where P_A is area normalised peak power density $\left(\approx \frac{V^2}{R_L \times A}\right)$ and *d* is the thickness of the active layer. By applying Eq. 3 to the measured output voltage responses (Fig. 4d-e), the progression of P_v vs. R_L were extracted from the present devices, as shown in Fig. 4f. From this, the calculated P_v for both devices can be seen increasing with increasing R_L. We note that the extracted P_v parameters are still lower than what can be expected, since the matching R_L for both devices clearly lay outside the current measurement setup. As shown in Fig. 4f, the extracted P_v of 4μW/cm^3 (pristine) and 16μW/cm^3 (thermally modified) strongly suggests that thermal modification of hydrothermally grown ZnO NWs enabled the NG to generate comparatively higher output power than the unmodified ZnO NW device.

Conclusions

The present work has demonstrated the growth of single crystalline ZnO nanowires (NWs) by the low temperature hydrothermal process at around 100^{o}C. Thermal annealing of such NWs at around 450^{o}C in ambient air has been shown to sufficiently reduce the excess free carriers . The suppression of the excess free carriers was verified by assessing the performance of single ZnO NW field-effect transistors and ZnO NW based piezoelectric nanogenerators. A single NW FET incorporating these thermally modified NWs was found to exhibit excellent field-effect transport behaviour that were unobtainable in as-grown NWs. This included low off-state current (pA range), high on-state current (~10μA at 5V drain bias), steep subthreshold slope (~600mV/dec), moderate field-effect mobility of ~10cm^2/V-s and an effective carrier concentration of ~3.7x10^{17}/cm^3. The fabricated NGs employed vertically oriented ZnO NW arrays on Au/Ti-Si substrates and ~7μm thick Polydimethylsiloxane (PDMS) polymer matrix. Assessment of a NG incorporating these thermally modified ZnO NWs revealed enhancements key device performance parameters compared to a reference device with pristine NWs. The thermally modified ZnO NWs device exhibited moderate peak output voltage of ~109mV and a power density of ~16μW/cm^3. This work may find practical application in several areas of hydrothermal ZnO nanomaterial research, including high performance single nanowire transistors and piezoelectric energy harvesters.

Acknowledgements

This work was funded by the Region Centre CEZnO project (Convertisseur Electromécanique à base de nanofils ZnO, 2011-2014). The Authors are grateful for the supports from MEPS-Flexible (2015-2018) and ANR FLEXIBLE projects (ANR-14-CE08-0010-01). The Authors are also grateful to the Labex GaNeX group for collaboration.

References

1 D. Elliott, R. E. Hester and R.M. Harrison, Editors. 2003, *R. Soc. of Chem*. p. 19-48.
2 R. Bogue, *Sens. Rev*. 2015, **35**, 1, 1-5.
3 S. P. Beeby, M. J. Tudor, N. M. White, *Meas. Sci. Technol*. 2006, **17**,12, R175.
4 H. Kim, J. -H. Kim, J. Kim, *Int. J. Precis. Eng. Man*. 2011, **12**, 6, 1129-1141.
5 G. Zhu, A. C. Wang, Y. Liu, Y. Zhou, Z. L. Wang, *Nano. Lett.* 2012, **12**, 6, 3086-3090.
6 J. Briscoe, N. Jalali, P. Woolliams, M. Stewart, P. M. Weaver, M. Cain, S. Dunn, *Energy Environ. Sci.* 2013, **6**, 10, 3035-3045.
7 S. Lee, S. -H. Bae, L. Lin, Y. Yang, C. Park, S. -W. Kim, S. N. Cha, H. Kim, Y. J. Park,Z. L. Wang, *Adv. Funct. Mater*. 2013, **23**, 19, 2445-2449.
8 Y. Hu, L. Lin, Y. Zhang, Z. L. Wang, Replacing a Battery by a Nanogenerator with 20 V Output. *Adv. Mater*. 2012, **24**, 1, 110-114.
9 L. Lin, Y. Hu, C. Xua, Y. Zhang, R. Zhanga, X. Wen, Z. L. Wang, *Nano Energy* 2013, **2**, 1, 75-81.
10 S. Lee, R. Hinchet, Y. Lee, Y. Yang, Z. -H. Lin, G. Ardila, L. Montès, M. Mouis, Z. L. Wang, *Adv. Funct. Mater*. 2014, **24**, 8, 1163-1168.
11 R. Hinchet, S. Lee, G. Ardila, L. Montès, M. Mouis, Z. L. Wang, Adv. Funct. Mater. 2014, **24**, 7, 971-977.
12 Z. L. Wang, *Adv. Mater*. 2012, **24**, 2, 280-285.
13 G. Zhu, R. Yang, S. Wang, Z. L. Wang, *Nano. Lett.* 2010, **10**, 8, 3151-3155.
14 K. Y. Lee, B. Kumar, J. -S. Seo, K. -H. Kim, J. I. Sohn, S. N. Cha, D. Choi, Z. L. Wang, S. -W. Kim, *Nano. Lett.* 2012, **12**, 4, 1959-1964.
15 M. Trejo, P. Santiago, H. Sobral, L. Rendón, U. Pal, *Cryst. Growth. Des*. 2009, **9**, 7, 3024-3030.
16 D. Kälblein, R. T. Weitz, H. J. Böttcher, F. Ante, U. Zschieschang, K. Kern, H. Klauk,*Nano. Lett.* 2011, **11**, 12, 5309-5315.
17 Tsividis Y. P. Operation and modeling of MOS transistor. 2nd ed. 1988, Singapore: McGraw-Hill.
18 J. Goldberger, D. J. Sirbuly, M. Law, P. Yang, J. Phys. Chem. B 2005, **109**, 1, 9-14.
19 C. Opoku, K. F. Hoettges, M. P. Hughes, V. Stolojan, S.R.P. Silva, M. Shkunov, *Nanotechnology* 2013, **24**, 40, 405203.
20 J. C. Lötters, W. Olthuis, P. H. Veltink, P. Bergveld, *J. Micromech. Microeng.* 1997, **7**, 3, 145.